



# The Electronic Structure of Lanthanide Impurities in TiO<sub>2</sub>, ZnO, SnO<sub>2</sub>, and Related Compounds

Pieter Dorenbos<sup>2</sup>

Delft University of Technology, Faculty of Applied Sciences, Department of Radiation Science and Technology (FAME-LMR), 2629 JB Delft, Netherlands

The vacuum referred binding energy of electrons in the 4f<sup>n</sup> levels for all divalent and trivalent lanthanide impurity states in TiO<sub>2</sub>, ZnO, SnO<sub>2</sub>, and related compounds MTiO<sub>3</sub> and MSnO<sub>3</sub> (M = Ca<sup>2+</sup>, Sr<sup>2+</sup>, Ba<sup>2+</sup>) and Ca<sub>2</sub>SnO<sub>4</sub> are presented. They are obtained by collecting data from the literature on the spectroscopy of lanthanide ions, and by combining that data with the chemical shift model. The model provides the energy at the top of the valence band and at the bottom of the conduction band, and it will be shown that those energies are in excellent agreement with what is known from techniques like photo-electron spectroscopy and electrochemical studies. Electronic level diagrams are presented that explain and predict aspects like absence or presence of lanthanide 4f-4f or 5d-4f emissions and the preferred lanthanide valence.

© 2013 The Electrochemical Society. [DOI: 10.1149/2.005403jss] All rights reserved.

Manuscript received October 17, 2013. Published December 20, 2013.

Recently the chemical shift model was introduced<sup>1</sup> for the lanthanide impurities in compounds. By using spectroscopic data for different lanthanides like Ce<sup>3+</sup>, Pr<sup>3+</sup>, Tb<sup>3+</sup>, Eu<sup>3+</sup>, Yb<sup>3+</sup> in the same compound, the model enables to derive the electronic structure with the absolute electron binding energies, i.e., relative to the energy of the electron at rest in vacuum, in all divalent and all trivalent lanthanides.<sup>2</sup> It has been applied to about 50 different compounds (fluorides, chlorides, aluminates, phosphates, borates etc.) and full consistency with available experimental data from different fields of science was demonstrated.<sup>2-4</sup> It was found that in inorganic compounds based on rare earth cations, like YPO<sub>4</sub> and LaBO<sub>3</sub>, and/or alkaline and/or alkaline earth cations like CaF<sub>2</sub> and CaGa<sub>2</sub>S<sub>4</sub>, the binding energy at the bottom of the conduction band  $E_C$  is typically near  $-2$  eV. Sc-based compounds like ScBO<sub>3</sub> and ScPO<sub>4</sub> tend to show lower values for  $E_C$  which was attributed to a large binding energy of electrons in the 3d-shell of Sc<sup>3+</sup>/Sc<sup>2+</sup> that forms the bottom of the conduction band.<sup>4</sup> In this work the model will be applied to TiO<sub>2</sub>, ZnO, SnO<sub>2</sub>, and related ternary compounds. The compounds were selected because of their high importance for many applications.

TiO<sub>2</sub> has been and still is thoroughly investigated for its photocatalytic activity and ability for photoelectrochemical water splitting.<sup>5</sup> The activity can be enhanced or modified by doping with transition metal or rare earth ions.<sup>6,7</sup> Much is already known on the electronic structure and properties of this compound in its various crystallographic appearances, i.e., rutile-TiO<sub>2</sub>, anatase-TiO<sub>2</sub>, and brookite-TiO<sub>2</sub>. Here we will focus on the anatase-phase. ZnO is an important member of the II-VI semiconductor family. An extensive review on the physical and optical properties of ZnO can be found in Ref. 8. At ambient conditions only the wurtzite phase is thermodynamically stable and all data and schemes in this work will pertain to that phase. SnO<sub>2</sub> has much in common with ZnO and TiO<sub>2</sub> regarding electronic structure. SnO<sub>2</sub> and Sn based compounds like InSnO<sub>3</sub> are well known transparent conducting oxides (TCO).<sup>9</sup>

## Methodology

The chemical shift is the shift of the electron binding energy from its free ion value toward lower (less negative) value by the coulomb repulsion with its chemical environment, and since the environment is formed by the coordination anion ligands, it are the properties of those ligands that are essential. The chemical shift model explains why only one chemical environment dependent parameter controls the location of all 4f levels of each divalent and each trivalent lanthanide. The coulomb repulsion energy  $U(6, A)$ , defined as the energy difference between the 4f-ground state of Eu<sup>2+</sup> and Eu<sup>3+</sup>, see arrow 1 in Fig. 1,

plays the role of that parameter. The following equation was proposed<sup>1</sup>

$$E_{4f}(7, 2+, A) = -24.92 + \frac{18.05 - U(6, A)}{0.777 - 0.0353U(6, A)} \quad [1]$$

where  $E_{4f}(7, 2+, A)$  is the vacuum referred binding energy (VRBE) of an electron in the 4f<sup>7</sup> ground state of Eu<sup>2+</sup> in the chemical environment denoted with symbol  $A$ , and  $-24.92$  eV is the VRBE in the free ion. The right hand term is then the size of the chemical shift tied to  $U(6, A)$ .  $U(6, A)$  appears to vary mildly with type of compound. For fluorides it has values around 7.5 eV, for oxides it is about 7.1 eV in phosphates like YPO<sub>4</sub> and decreases with weaker bonding strength of the ligand electrons to values around 6.5 for compounds like La<sub>2</sub>O<sub>3</sub> and 6.3 eV for GaN. A convenient method to estimate  $U(6, A)$  is to use Ce<sup>3+</sup> as a probe ion. The average energy, or centroid energy, of the five possible 4f-5d transitions is known for 150 different compounds and it appears correlated with the size of  $U(6, A)$ .<sup>10</sup> Since the electronegativity  $\chi$  of a cation is a direct measure for how strong it will bond an anion ligand,<sup>11</sup> one may use electronegativity to estimate the centroid energy and  $U(6, A)$ . A higher weighted average cation electronegativity will increase both the centroid energy and  $U(6, A)$ . Longer bondlength has similar effect. In the case of TiO<sub>2</sub>, ZnO, and SnO<sub>2</sub> we deal with oxygen ligands that are bonded by either Ti<sup>4+</sup>, Zn<sup>2+</sup> or Sn<sup>4+</sup> that have  $\chi$  of 1.54, 1.65, and 1.80, respectively.<sup>11</sup> For example YAlO<sub>3</sub> has  $\chi_{av} = 1.42$  and  $U(6, A) = 6.81$  eV, and YBO<sub>3</sub> has  $\chi_{av} = 1.63$  and  $U(6, A) = 6.85$  suggesting that TiO<sub>2</sub> and ZnO will have similar value. Considering that Ti<sup>4+</sup>, Zn<sup>2+</sup>, and Sn<sup>4+</sup> are smaller than Y<sup>3+</sup>, bondlengths around a lanthanide on those sites will be smaller too resulting in smaller centroid energy and  $U(6, A)$ . We therefore estimate for TiO<sub>2</sub> and ZnO  $U(6, A) \approx 6.7$  eV and for SnO<sub>2</sub> with the larger value for  $\chi$   $U(6, A) \approx 6.8$  eV. Figure 1 shows the VRBE for all lanthanide states when a value of 6.7 eV is used for  $U(6, A)$ . The ground state energies for the lanthanides follow characteristic zigzag patterns, and the excited 4f<sup>n</sup>-states follow the Dieke diagram. The only thing that is further needed is to place the valence band and conduction band in the scheme to arrive at a full VRBE level diagram.

From studies with photoelectron spectroscopy, electrochemical cells or with electric studies (Schottky barrier) data is available on  $E_V$  and  $E_C$  in TiO<sub>2</sub>, ZnO, and SnO<sub>2</sub>. However, data are not consistent. The works by Refs. 5, 12–14 for example report for  $E_V$  in anatase-TiO<sub>2</sub> values of  $-7.2$ ,  $-7.8$ ,  $-7.5$ , and  $-7.0$  eV, respectively and for  $E_C$   $-4.0$ ,  $-4.6$ ,  $-4.3$ , and  $-4.0$  eV, respectively. The lines drawn in Fig. 1 at  $-4.2$  eV and  $-7.4$  eV represent the average values from those reports. ZnO is electronically very similar to anatase-TiO<sub>2</sub>. It has about the same bandgap and the same value for  $E_V$ ; in Ref. 12  $E_V$  is reported about 0.1 eV higher (less negative) but in Ref. 5 about 0.1 eV more negative. Therefore the scheme of Fig. 1 also applies as first approximation to ZnO.

<sup>2</sup>E-mail: p.dorenbos@tudelft.nl

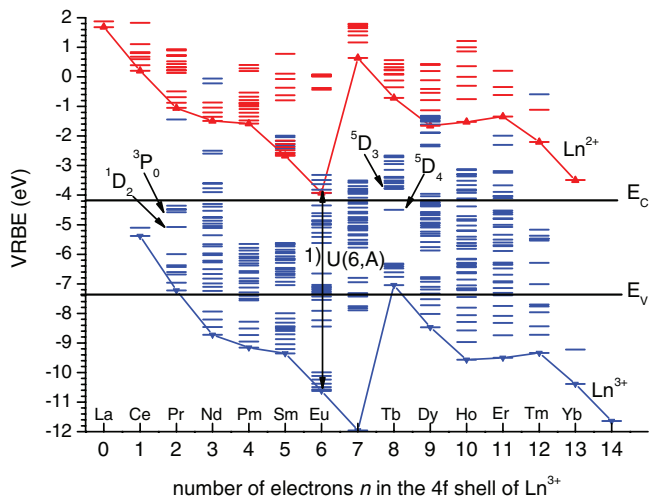


**Figure 1.** A first guess on the VRBE scheme that applies to anatase-TiO<sub>2</sub> and wurzite ZnO using  $U(6, A)$  is 6.7 eV. The lower zigzag curve with excited state levels pertains to Ln<sup>3+</sup> and the upper one to Ln<sup>2+</sup>.

We wish to seek confirmation of those energies or provide better values by using the chemical shift model. A method that works for wide bandgap insulators is to seek for information on the energy of electron or charge transfer  $E^{CT}(6, 3+, A)$  from the valence band to Eu<sup>3+</sup>. It provides a good measure for the location  $E_{4f}(7, 2+, A)$  of the Eu<sup>2+</sup> ground state above  $E_V(A)$

$$E_V(A) = E_{4f}(7, 2+, A) - E^{CT}(6, 3+, A), \quad [2]$$

then when also the energy  $E^{ex}(A)$  of exciton creation is known one obtains the location of the bottom of the conduction band

$$E_C(A) = E_V(A) + E^{ex}(A) + E_{e-h}^{ex}(A) \equiv E_X(A) + E_{e-h}^{ex}(A) \quad [3]$$

where one has to add the electron and hole binding energy  $E_{e-h}^{ex}(A)$  of the exciton state to reach the conduction band bottom. Figure 1 illustrates already for TiO<sub>2</sub> but also for many other compounds in this work that the energy for charge transfer to Eu<sup>3+</sup> is larger than or very close to the bandgap energy. An Eu<sup>3+</sup> charge transfer band in spectra is then obscured by intense host lattice absorption bands. One has to rely on other spectroscopic data to place  $E_V$  and  $E_X$ .

Figure 1 shows that Ce<sup>3+</sup>, Pr<sup>3+</sup>, and Tb<sup>3+</sup> have a ground state located within the bandgap, and for those three lanthanides one may observe an electron transition from the 4f ground state directly into the conduction band which is also known as intervalence charge transfer (IVCT). It provides data on level location relative to the conduction band. Figure 1 shows that the <sup>3</sup>P<sub>0</sub>-level of Pr<sup>3+</sup> and the <sup>5</sup>D<sub>3</sub> and <sup>5</sup>D<sub>4</sub> levels of Tb<sup>3+</sup> are located close to  $E_C$ . When a level is located above, emission from such level will not be observed due to auto-ionization to conduction band states, and if just below emission will be quenched at relatively low temperature. Therefore absence or presence, and the quenching temperature of 4f-4f emission lines, also provide information on where to place  $E_C$ .

In this work we will first estimate  $U(6, A)$ .  $E^{ex}$  is obtained from experimental data on the fundamental absorption threshold and the energy of host exciton creation. Since  $E^{ex}$  tends to increase slightly with lowering of temperature, we will always provide the values, or best estimates, that pertain to low temperature, say 10 K. The value for  $E_{e-h}^{ex}$  in wide bandgap (>6 eV) compounds with small dielectric constant where excitons tend to be of Frenkel exciton type is taken about 8% of the value for  $E^{ex}$ .<sup>15</sup> In high dielectric constant compounds that tend to have smaller band gaps, the excitons are usually of the Wannier exciton type with smaller binding energy. Sometimes values are known from experiment, in other cases an estimated or typical value will be used. Next information on Eu<sup>3+</sup> luminescence excitation spectra is collected. Occasionally values, or approximate values, for  $E^{CT}$  can be derived. If a CT band is not observed it indicates

**Table I. Experimental input data for construction of VRBE schemes. All energies are in eV. Estimated or deduced values are in italics. IVCT and CT energies pertain to Pr<sup>3+</sup> and Eu<sup>3+</sup>.**

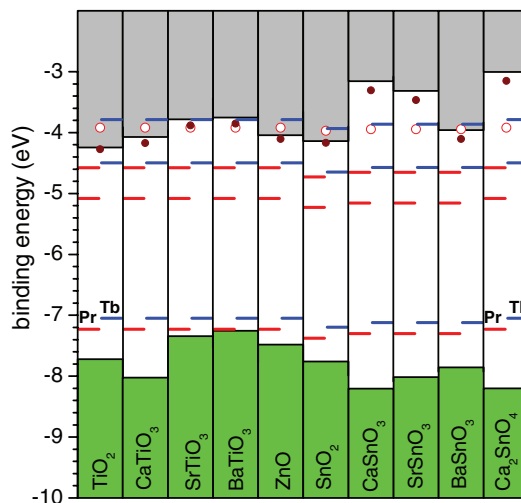
A	$E^{ex}$	$E_{e-h}^{ex}$	$E^{IVCT}$	$E^{CT}$	$U(6, A)$	$E_V$
anatase-TiO <sub>2</sub>	3.45	0.03		3.8	6.7	-7.72
CaTiO <sub>3</sub>	3.85	0.1	3.25	4.1	6.7	-8.02
SrTiO <sub>3</sub>	3.46	0.1	3.54	3.42	6.7	-7.34
BaTiO <sub>3</sub>	3.40	0.1	3.57	3.33	6.7	-7.25
ZnO	3.38	0.06		3.56	6.7	-7.48
SnO <sub>2</sub>	3.59	0.032		3.79	6.8	-7.76
CaSnO <sub>3</sub>	4.90	0.15		4.26	6.75	-8.21
SrSnO <sub>3</sub>	4.55	0.15		4.07	6.75	-8.01
BaSnO <sub>3</sub>	3.75	0.15		3.9	6.75	-7.86
Ca <sub>2</sub> SnO <sub>4</sub>	5.05	0.15		4.28	6.70	-8.20

that  $E_{4f}(7, 2+, A) > E_X(A)$ . For Pr<sup>3+</sup> we will use information on IVCT energies and presence/absence and quenching temperature of the emission from the <sup>3</sup>P<sub>0</sub> level. For Tb<sup>3+</sup> we will use likewise information on IVCT and presence/absence and quenching temperature of the emission from <sup>5</sup>D<sub>3</sub> and <sup>5</sup>D<sub>4</sub> levels. Occasionally one may use the onset of charge transfer from the top of the valence band to Ce<sup>4+</sup> as an indication for the location of the Ce<sup>3+</sup> ground state. By combining all bits and pieces of information on different lanthanides in the same host, the most likely values for  $U(6, A)$ ,  $E_X$ , and  $E_V$  will be proposed.

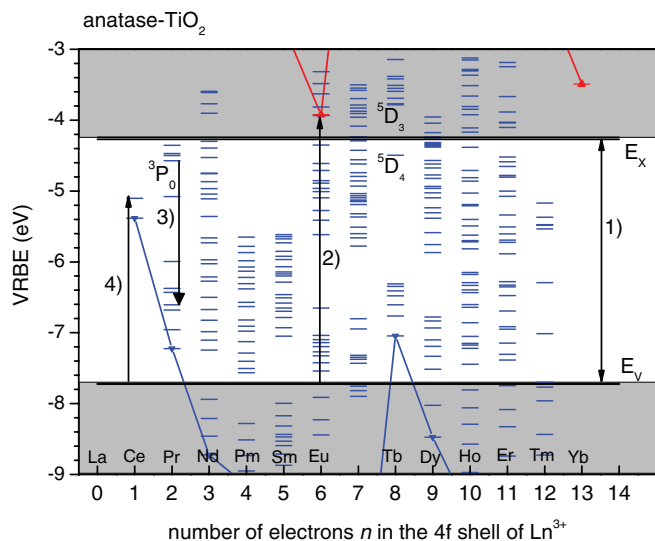
## Results

Table I compiles data derived from spectroscopy that are sufficient to construct a complete VRBE scheme as in Fig. 1. Fig. 2 overviews the results in a so-called stacked band diagram. It shows how the binding energy at the top of the valence band and the bottom of the conduction band changes with type of compound. For each compound on the left the <sup>3</sup>H<sub>4</sub> ground state and <sup>1</sup>D<sub>2</sub> and <sup>3</sup>P<sub>0</sub> excited state levels of Pr<sup>3+</sup> are shown. For each compound on the right the <sup>7</sup>F<sub>6</sub> ground state and <sup>5</sup>D<sub>4</sub> and <sup>5</sup>D<sub>3</sub> excited states level of Tb<sup>3+</sup> are shown. The data points for each compound are  $E_X$  and the Eu<sup>2+</sup> ground state energy  $E_{4f}(7, 2+, A)$ . An account on how all data was obtained, derived, or estimated follows below.

*anatase-TiO<sub>2</sub>.*—Figure 3 shows the VRBE scheme for anatase-TiO<sub>2</sub> from the data in Table I. The use of  $U(6, A) = 6.7$  eV was motivated in the previous section. The optical bandgap or absorption threshold of 3.2 eV is well known<sup>16</sup> and  $E^{ex}$  is 3.45 eV,<sup>17-19</sup> see arrow 1). A value of 30 meV is estimated for  $E_{e-h}^{ex}$ . For Eu<sup>3+</sup> in thin film TiO<sub>2</sub>, an absorption band at 3.75 eV was assigned to the  $E^{CT}(6, 3+, A)$  excitation by



**Figure 2.** The stacked VRBE schemes together with relevant Pr<sup>3+</sup> levels on the left and Tb<sup>3+</sup> levels on the right. Open circle data points are the location of the Eu<sup>2+</sup> ground state level and closed circle data points are  $E_X$ .



**Figure 3.** The VRBE scheme for anatase-TiO<sub>2</sub>.

Ref. 20 suggesting that the Eu<sup>2+</sup> ground state is located inside the conduction band. Similarly Luo et al.<sup>21</sup> attributes a small hump at 3.6 eV in the 10 K excitation spectrum to  $E^{CT}(6, 3+, A)$ . In Fig. 3  $E^{CT}$  was chosen 3.8 eV, see arrow 2). Kaczkan et al.<sup>22</sup> does not observe any Pr<sup>3+</sup> 4f-4f emission, and Amlouk et al.<sup>23</sup> show that the emission from the <sup>3</sup>P<sub>0</sub> level to <sup>3</sup>H<sub>6</sub> and <sup>3</sup>F<sub>4</sub> (arrow 3) in 20-30 nm sized TiO<sub>2</sub> starts to quench above 70K. Such low quenching temperature implies that the <sup>3</sup>P<sub>0</sub> level is located close below  $E_X$ ; in Fig. 3 and Fig. 2 it is 0.3 eV below. Moon et al.<sup>24</sup> does not observe any Tb<sup>3+</sup> emission down to 13 K in TiO<sub>2</sub> which agrees with the scheme where the Tb<sup>3+</sup> <sup>5</sup>D<sub>3</sub> level is inside and the <sup>5</sup>D<sub>4</sub> level is only 0.2 eV below  $E_X$ .

The Ce<sup>3+</sup> ground state in Fig. 3 is located above mid bandgap energy; 2.34 eV above  $E_V$ . Under such circumstance the Ce<sup>4+</sup> valence state is likely to occur<sup>25</sup> creating an electron acceptor state at 2.34 eV above  $E_V$ . It is indeed well established that Ce<sup>4+</sup> is stable in TiO<sub>2</sub>.<sup>6,26</sup> It induces a yellow color due to an absorption band that starts near 480 nm (2.6 eV) and continually increases toward the fundamental host absorption onset at 365 nm (3.4 eV).<sup>6,27</sup> The transition onset is indicated by arrow 4) in Fig. 3. In Ref. 4 it was found that for various oxide compounds the onset of valence band to Ce<sup>4+</sup> electron transfer is a good measure for the location of the Ce<sup>3+</sup> ground state above  $E_V$ . 2.6 eV is only slightly larger than 2.34 eV. In compounds like CeTiO<sub>4</sub> and CeTi<sub>2</sub>O<sub>6</sub> the charge transfer to Ce<sup>4+</sup> starts also at 500 nm (2.5 eV)<sup>28</sup> and the VRBE scheme for these compounds will be quite similar as that of anatase-TiO<sub>2</sub>.

*CaTiO<sub>3</sub>, SrTiO<sub>3</sub>, and BaTiO<sub>3</sub>.*—A host referred binding energy scheme (HRBE) scheme for CaTiO<sub>3</sub> with location of the ground state levels of the trivalent lanthanides relative to the top of the valence band was presented in Ref. 29. Figure 4 shows the VRBE scheme using the data from Table I. Compared to TiO<sub>2</sub>, the electronegativity  $\chi_{av}$  = 1.0 for Ca lowers  $\chi_{av}$  to 1.36 which is the same as that of LaAlO<sub>3</sub> with  $U(6, A) = 6.67$  eV,<sup>4</sup> and since the ionic radius of Ca<sup>2+</sup> and La<sup>3+</sup> are similar,  $U(6, CaTiO_3) = 6.7$  eV will be used. The room temperature absorption and luminescence excitation maximum is observed near 333 nm (3.72 eV)<sup>30-32</sup> and we will use 3.85 eV for  $E^{ex}(A)$  at 10 K (arrow 1). Eu<sup>3+</sup> doped CaTiO<sub>3</sub> does not show any evidence for a CT band<sup>33</sup> suggesting that  $E^{CT} > E_X$  (see arrow 2). The Pr<sup>3+</sup> IVCT band is well observed at 380 nm (3.25 eV, see arrow 3),<sup>30,32,34</sup> and this forms the most important parameter to construct the VRBE scheme. The binding energies with respect to the conduction band are almost the same as in TiO<sub>2</sub>, and like in TiO<sub>2</sub> emission from the <sup>3</sup>P<sub>0</sub> level of Pr<sup>3+</sup> or the <sup>5</sup>D<sub>3</sub> and <sup>5</sup>D<sub>4</sub> levels of Tb<sup>3+</sup> are not observed at room temperature.<sup>35</sup>

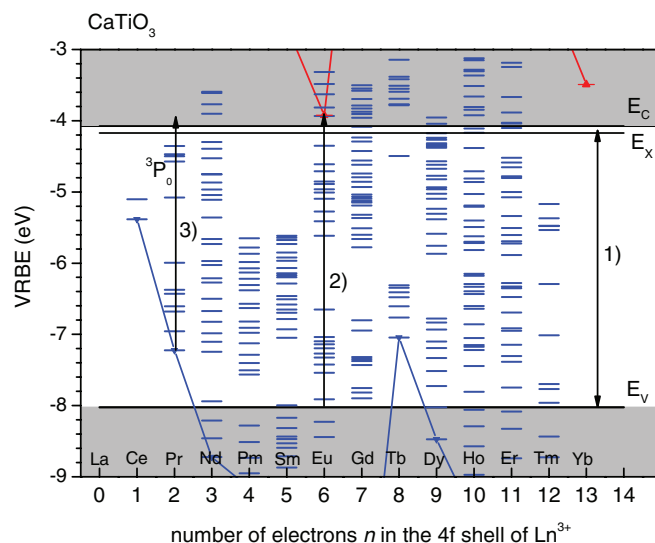


**Figure 4.** The VRBE scheme for CaTiO<sub>3</sub>.

For SrTiO<sub>3</sub>, and BaTiO<sub>3</sub> again  $U(6, A) = 6.7$  eV is chosen. The absorption onset in SrTiO<sub>3</sub> is at 3.27 eV<sup>36-38</sup> and excitons are created at  $E^{ex} = 3.46$  eV (360 nm).<sup>36,38</sup> BaTiO<sub>3</sub> has the same optical bandgap as SrTiO<sub>3</sub> in 39. A comparison of optical reflection and excitation spectra for CaTiO<sub>3</sub>, SrTiO<sub>3</sub>, and BaTiO<sub>3</sub> in Ref. 40 suggest however slightly smaller  $E^{ex} = 3.4$  eV in BaTiO<sub>3</sub>. In SrTiO<sub>3</sub> there are clear indications for the start of the Eu<sup>3+</sup> CT-band just before it is cutoff by host lattice absorption below 375 nm (3.30 eV).<sup>41</sup> In both SrTiO<sub>3</sub> and BaTiO<sub>3</sub> a Pr<sup>3+</sup> IVCT band is absent<sup>41,42</sup> and following the reasoning by Boutinaud et al.<sup>43</sup> the <sup>3</sup>H<sub>4</sub> Pr<sup>3+</sup> ground state must be close above or even inside the valence band. The Pr<sup>3+</sup> <sup>1</sup>D<sub>2</sub> emission dominates in CaTiO<sub>3</sub> and on diluting the compound with Sr<sup>2+</sup> the <sup>3</sup>P<sub>0</sub> emission appears until it fully dominates the emission in pure SrTiO<sub>3</sub> where it starts to quench around room temperature.<sup>38,43</sup> Clearly  $E_C$  must increase on diluting with Sr<sup>2+</sup>. By choosing  $E^{CT} = 3.42$  eV for SrTiO<sub>3</sub> and 3.33 eV for BaTiO<sub>3</sub> VRBE schemes and the band locations as in Fig. 2 are obtained consistent with all those observations.

*wurtzite-ZnO.*—The first HRBE scheme for ZnO based on lanthanide spectroscopy data was presented in Ref. 44. Since appearance of that work better parameters to construct HRBE schemes became available<sup>29</sup> and a renewed evaluation will be made here. The VRBE scheme made with the data collected in Table I is shown in Fig. 5. The bandgap of ZnO is well established. The  $n = 1$  Wannier exciton peak is at 3.38 eV with an exciton binding energy of 60 meV.<sup>8,45,46</sup>

Excitation spectra of Eu<sup>3+</sup> emission reported by Refs. 47, 48 do not show any evidence for a CT band below the fundamental absorption onset. A shoulder at 355 nm (3.5 eV) on the high energy side of the host absorption peak might be a signal from the Eu<sup>3+</sup> CT-band<sup>49</sup> consistent with (see arrow 3) the proposed scheme of Fig. 5. The emission from Pr<sup>3+</sup> at room temperature is dominated by the 630 nm <sup>3</sup>P<sub>0</sub> → <sup>3</sup>H<sub>4</sub> emission (arrow 2).<sup>50</sup> The same emission in TiO<sub>2</sub> starts to quench above 70 K. This suggests that  $E_X$  is somewhat further above the <sup>3</sup>P<sub>0</sub> level than in TiO<sub>2</sub>. For Tb<sup>3+</sup> doped ZnO, emission from <sup>5</sup>D<sub>3</sub> is, as expected, not observed, and that from <sup>5</sup>D<sub>4</sub> is observed (see arrow 4) at 7 K.<sup>51</sup>

The scheme places the Ce<sup>3+</sup> ground state at 2.1 eV above  $E_V$  (arrow 5) which implies that, like for anatase-TiO<sub>2</sub>, Ce can exist in the 4+ valence state. Indeed several reports can be found on the synthesis, spectroscopic properties, and valence state of Ce<sup>4+</sup> doped ZnO nanorods, nanowires, and nanocages.<sup>52-54</sup>

*SnO<sub>2</sub>.*—The VRBE scheme for SnO<sub>2</sub> using the data in Table I is shown in Fig. 6. The excitation spectrum of intrinsic luminescence shows a hydrogen like series of excitonic lines with the first exciton peak at 3.6 eV and with an exciton binding energy of 32 meV.<sup>55</sup> Excitation

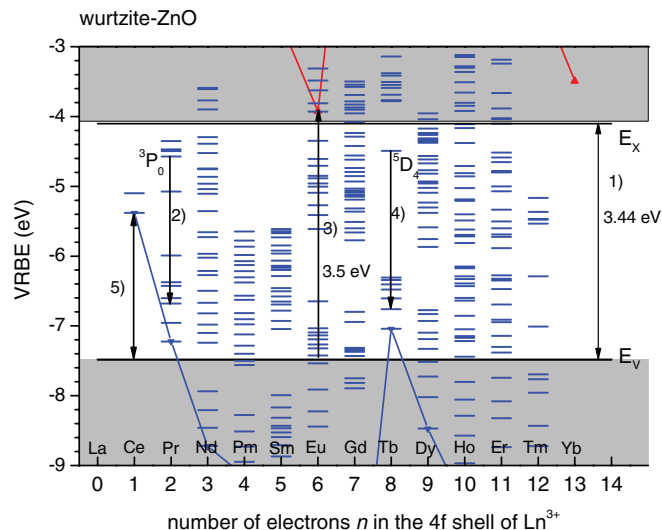


Figure 5. The VRBE scheme for wurtzite-ZnO.

spectra of  $\text{Eu}^{3+}$  emission in  $\text{SnO}_2$  reveal an intense excitation band around the host excitation<sup>56-59</sup> which provides a lower bound on the CT-band energy of  $\text{Eu}^{3+}$ , see arrow 1 in Fig. 6. Spectroscopic information on  $\text{Pr}^{3+}$  was not found in the literature. Like in  $\text{TiO}_2$  and  $\text{ZnO}$  there is no emission from the  $\text{Tb}^{3+}$   $^5D_3$  level<sup>60</sup> indicating that it is located above  $E_x$ . Emission from the  $^5D_4$  level (see arrow 2) is observed in thin film  $\text{SnO}_2$  and in single crystal  $\text{SnO}_2$ . It starts to quench above 170 K, and at room temperature it has dropped to 60% of its low temperature intensity.<sup>61,62</sup> Since the  $\text{Tb}^{3+}$   $^5D_4$  emission appears more temperature stable than in  $\text{CaTiO}_3$ , the  $^5D_4$  level is most likely located further below  $E_C$ . By taking  $E^{CT} = 3.79$  eV, the schemes in Fig. 6 and Fig. 2 are obtained that are best consistent with above spectroscopic data.

*CaSnO<sub>3</sub>, SrSnO<sub>3</sub>, BaSnO<sub>3</sub>, and Ca<sub>2</sub>SnO<sub>4</sub>.*—For  $\text{CaSnO}_3$   $\chi_{av} = 1.53$ , and we will use  $U(6, A) = 6.75$  eV which falls in between the value for  $\text{SnO}_2$  and  $\text{TiO}_2$ . The same values will be adopted for  $\text{SrSnO}_3$  and  $\text{BaSnO}_3$ . From the luminescence excitation and absorption maxima of undoped and rare earth doped  $\text{CaSnO}_3$ <sup>63-66</sup> we obtain  $E^{ex} = 4.9$  eV at 10 K. The  $\text{Eu}^{3+}$  excitation band is clearest observed in the work by Fu et al.<sup>67,68</sup> giving on average  $E^{CT}$  is 4.26 eV. The resulting band diagram in Fig. 2 shows a much higher lying conduction band as  $\text{SnO}_2$ . It predicts very temperature stable  $\text{Pr}^{3+}$   $^3P_0$  and  $\text{Tb}^{3+}$   $^5D_4$  emission.

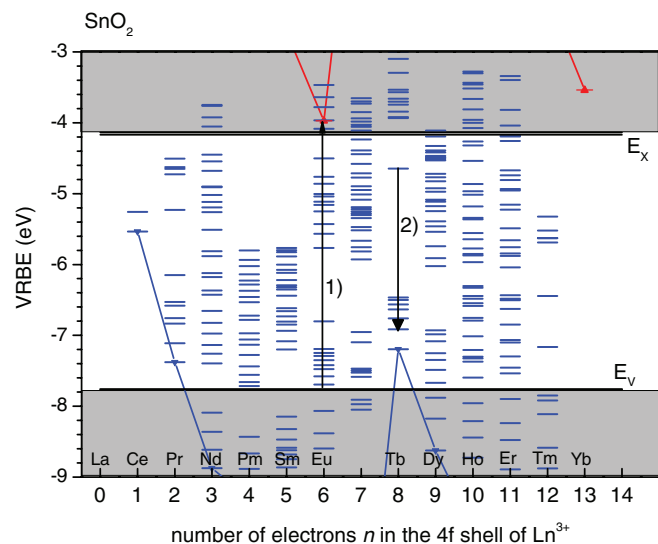


Figure 6. The VRBE scheme for  $\text{SnO}_2$ .

Indeed at room temperature the emission from the  $^3P_0$  level of  $\text{Pr}^{3+}$  dominates<sup>66,69</sup> and the  $^5D_4$  emission from  $\text{Tb}^{3+}$  is temperature stable up to 350 K.<sup>65</sup>

Information on  $\text{SrSnO}_3$  is less abundant than on  $\text{CaSnO}_3$ . Diffuse reflection spectra indicate that  $E^{ex}$  is about 0.35 eV smaller than in  $\text{CaSnO}_3$ ,<sup>63</sup> and excitation and absorption spectra reveal host related maxima at 280 nm.<sup>70,71</sup> From this a low temperature  $E^{ex}(10K) = 4.55$  eV is derived. The CT-band energy of 4.07 eV is from.<sup>70</sup> With this data Figure 2 shows that  $E_C$  is significantly lower than in  $\text{CaSnO}_3$ . At room temperature  $\text{Tb}^{3+}$  emission from  $^5D_4$  is observed but not from  $^5D_3$ .<sup>71,72</sup> Information on  $\text{Pr}^{3+}$  spectroscopy was not found. The fundamental absorption in  $\text{BaSnO}_3$  is about 1.3 eV smaller than in  $\text{CaSnO}_3$ ,<sup>63</sup> and Ref. 73 finds in thin film  $\text{Ba}_{1-x}\text{Sr}_x\text{SnO}_3$  a fundamental absorption edge shifting from 3.49 eV in  $\text{BaSnO}_3$  to 4.27 eV in  $\text{SrSnO}_3$ . A value of 3.75 eV will be used for  $E^{ex}(LT)$  in  $\text{BaSnO}_3$ . There appears no information on  $\text{Eu}^{3+}$ ,  $\text{Pr}^{3+}$ , and  $\text{Tb}^{3+}$  spectroscopy that can be used to place  $E_V$  and  $E_C$ . Weifeng Zhang et al.<sup>63</sup> presented  $E_V$  and  $E_C$  for Ca-, Sr-, and  $\text{BaSnO}_3$  determined with a semi-empirical approach. By choosing  $E^{CT} = 3.9$  eV for  $\text{BaSnO}_3$  a best agreement between the band positions in Fig. 2 with those in Ref. 63 is obtained.

$\text{Ca}_2\text{SnO}_4$  was added to our study to see how further increase of  $\text{CaO}$  content in  $\text{SnO}_2$  affects the electronic structure.  $\chi_{av} = 1.40$  for  $\text{Ca}_2\text{SnO}_4$  which is close to that of  $\text{CaTiO}_3$  and the same value of 6.7 eV for  $U(6, A)$  will be used.  $E^{ex}(LT) = 5.05$  eV is based on absorption and luminescence excitation spectra in Refs. 74, 75, and  $E^{CT} = 4.28$  eV is reasonably reliable obtained from.<sup>74,76-78</sup>

## Discussion

One may confirm the results on  $E_V$  and  $E_C$  in Table I and Fig. 2 by using data from independent techniques. In section II it was mentioned that reports on  $E_V$  for anatase  $\text{TiO}_2$  range from  $-7.0$  to  $-7.8$  eV which is to be compared with the value of  $-7.7$  eV found in this work. In 1967 Svank reported<sup>79</sup> a photo-electron emission threshold of 7.82 eV for  $\text{ZnO}$  to be compared with  $-7.48$  eV in this work. In the case of n-type  $\text{ZnO}$  the work function or electron affinity is equivalent to the energy at the bottom of the conduction band, and values reported in literature are in the  $-3.5$  to  $-5.2$  eV range<sup>80-82</sup> to be compared with  $-4.0$  eV in this work. Reports on  $\text{SnO}_2$  for  $E_V$  and  $E_C$  are  $-7.7$  eV and  $-4.30$  eV in Ref. 83,  $-8.24$  eV and  $-4.44$  eV in Ref. 12,  $-8.4$  eV and  $-4.9$  eV in Ref. 5, and  $-8.2$  eV and  $-4.6$  eV in Ref. 14. These values should be compared with the higher values of  $-7.76$  eV and  $-4.14$  eV found in this work.

The advantage of the methodology of this work is that  $E_V$  and  $E_C$  can be quite easily obtained for a large amount of compounds enabling to compare the electronic structure diagrams of different compounds with each other, and although also this methodology will have its error that error will be largely systematic. With schemes as in Fig. 2, even with unknown systematic error, one may look for trends in  $E_V$  and  $E_C$  with type of compound. Once trends are established and knowledge on its origins even more reliable schemes together with predictive tools can be developed. For example one observes that  $E_V$  and  $E_C$  for  $\text{TiO}_2$  and  $\text{SnO}_2$  are quite similar. Adding  $\text{CaO}$  to the compounds to form  $\text{CaTiO}_3$  and  $\text{CaSnO}_3$  one observes that  $E_V$  lowers and  $E_C$  rises. If next the size of the cation increases  $\text{Ca} \rightarrow \text{Sr} \rightarrow \text{Ba}$ , the energy of the valence band increases. This is quite common behavior also observed for many wide bandgap insulators.<sup>2</sup> A larger bondlength reduces the attractive coulomb interaction between cation and anion and consequently the electron binding of anion electrons decreases and that of cation electrons increases resulting in a rising of the valence band and a lowering of the conduction band. A phenomenon also known as the Madelung effect. The conduction band however in ternary compounds is formed by the orbitals of both type of cations. For the iso-structural  $\text{MTiO}_3$  compounds, Fig. 2 shows that  $E_C$  increases with larger sized  $M^{2+}$  contrary to what is expected from the Madelung effect. In those compounds the bottom of the conduction band is formed by  $\text{Ti}^{3+}$   $3d^1$  orbitals tetrahedrally coordinated by oxygen ligands. This can be explained with another effect. The larger bondlength reduces the 10Dq

splitting of the  $Ti^{3+} 3d^1$  levels causing a rising of  $E_C$  with larger sized  $M^{2+}$ . For the  $MSnO_3$  compounds there is no such crystal field splitting effect. Here the conduction band is formed by the 5s orbitals of  $Sn^{3+}$  and the 4s, 5s, or 6s orbital of  $M^{2+}$  that are not subject to crystal field splitting. Comparing  $SnO_2$ ,  $CaSnO_3$ , and  $Ca_2SnO_4$ , one observes that with increase of CaO content  $E_V$  lowers and  $E_C$  rises. The conduction band bottom is more and more dominated by  $Ca^{2+} 4s$  orbitals that are located at higher energy than the  $Sn^{4+} 5s$  orbitals thus rising  $E_C$ . The electronegativity of Ca is smaller than that of Sn suggesting weaker bonding of the oxygen ligands. Yet the valence band binding energy becomes stronger with Ca content. Possibly both ionic bonding and covalent bonding should be considered and more definite answers can be supplied when band structure calculation are available.

## Conclusions

The electronic structure scheme for the lanthanides in  $TiO_2$ ,  $ZnO$ , and  $SnO_2$  and related compounds were derived from lanthanide spectroscopy by using the chemical shift model. Vacuum referred binding energies for the valence band and conduction band electrons are obtained that are consistent with what is known in literature. This demonstrates that the chemical shift model that was already verified for fluorides and many wide bandgap oxide compounds applies also for compounds with low lying conduction band energies. In compounds with  $E_C$  close to  $-4$  eV, all divalent lanthanide ground state energies are inside the conduction band. Divalent lanthanides cannot exist in those type of compounds, and an  $Eu^{3+}$  charge transfer band will be obscured by host lattice transitions. The lowest 5d-states of trivalent lanthanides will be located inside the conduction band preventing any 5d-4f emission. The  $Pr^{3+} 3P_0$  and  $Tb^{3+} 5D_3$  and  $5D_4$  levels are close to  $E_C$ , and the absence or presence of emission from these levels provide good indicators for the approximate location of  $E_C$ . Together with observation of IVCT bands enough information can be gathered to construct a VRBE binding energy scheme as in Fig. 2.

## References

- P. Dorenbos, *Phys. Rev. B*, **85**, 165107 (2012).
- P. Dorenbos, *Phys. Rev. B*, **87**, 035118 (2013).
- P. Dorenbos, *J. Lumin.*, **136**, 122 (2013).
- P. Dorenbos, *J. Phys.: Condens. Matter*, **25**, 225501 (2013).
- T. Bak, J. Nowotny, M. Rekas, and C. C. Sorrell, *Int. J. Hydrogen Energy*, **27**, 991 (2002).
- Noor Aman, P. K. Satapathy, T. Mishra, M. Mahato, and N. N. Das, *Mat. Res. Bull.*, **47**, 179 (2012).
- Wan-Jian Yin, Houwen Tang, Su-Huai Wei, Mowafak M. Al-Jassim, J. Turner, and Yanfa Yan, *Phys. Rev. B*, **82**, 045106 (2010).
- U. Ozgur, Ya. I. Alivov, C. Liu, A. Teke, M. A. Reshchikov, S. Dogan, V. Avrutin, S. J. Cho, and H. Morkoc, *J. Appl. Phys.*, **98**, 041301 (2005).
- K. Ellmer, *Nature Photonics*, **6**, 809 (2012).
- P. Dorenbos, *J. Lumin.*, **135**, 93 (2013).
- J. Malito, *Chimica Oggi - Chemistry Today*, **13**, 57 (1995).
- P. Tiwana, P. Docampo, M. B. Johnston, H. J. Snaith, and L. M. Herz, *ACS Nano*, **5**, 5158 (2011).
- P. A. Kohl, S. N. Frank, and A. J. Bard, *J. Electrochem. Soc.*, **124**, 225 (1977).
- M. Miyauchi, A. Nakajima, T. Watanabe, and K. Hashimoto, *Chem. Mater.*, **14**, 2812 (2002).
- P. Dorenbos, *J. Phys.: Condens. Matter*, **15**, 8417 (2003).
- R. Lopez and R. Gomez, *J. Sol-Gel Sci. Technol.*, **61**, 1 (2012).
- H. Tang, F. Levy, H. Berger, and P. E. Schmid, *Phys. Rev. B*, **52**, 7771 (1995).
- Yuechan Cao, Zongyan Zhao, Juan Yi, Chenshuo Ma, Dacheng Zhou, Rongfei Wang, Chen Li, and Jianbei Qiu, *J. Alloys and Comp.*, **554**, 12 (2013).
- K. Madhusudan Reddy, S. V. Manorama, and A. Ramachandra Reddy, *Mat. Chemistry and Physics*, **78**, 239 (2002).
- A. Podhorodecki, G. Zatyryb, P. Sitarek, J. Misiewicz, D. Kaczmarek, J. Domaradzki, A. Borkowska, and E. L. Proclow, *Thin Solid Films*, **517**, 6331 (2009).
- Wenqin Luo, Renfu Li, Guokui Liu, M. R. Antonio, and Xueyuan Chen, *J. Phys. Chem. C*, **112**, 10370 (2008).
- M. Kaczkan, D. A. Pawlak, S. Turczynski, and M. Malinowski, *Opt. Mater.*, **33**, 1519 (2011).
- A. Amlouk, L. El Mir, S. Kraiem, M. Saadoun, S. Alaya, and A. C. Pierre, *Mat. Science and Engin. B*, **146**, 74 (2008).
- Byung Kee Moon, Jung Hyun Jeong, Soung-soo Yi, Sung Chul Kim, Haeyoung Choi, and Jung Hwan Kim, *Opt. Mater.*, **28**, 676 (2006).
- P. Dorenbos, *J. Mater. Chem.*, **22**, 22344 (2012).
- J. Zhang, W. Peng, Z. Chen, H. Chen, and L. Han, *J. Phys. Chem. C*, **116**, 19182 (2012).
- Vaclav Stengl, Snezana Bakardjieva, and Nataliya Murafa, *Mater. Chem. Phys.*, **114**, 217 (2009).
- S. Otsuka-Yao-Matsuo, T. Omata, and M. Yoshimura, *J. Alloys Comp.*, **376**, 262 (2004).
- P. Dorenbos, A. H. Krumpel, E. van der Kolk, P. Boutinaud, M. Bettinelli, and E. Cavalli, *Optical Materials*, **32**, 1681 (2010).
- Xianmin Zhang, Jiahua Zhang, Meiyuan Wang, X. Zhang, H. Zhao, and Xiao-Jun Wang, *J. Lumin.*, **122-123**, 958 (2007).
- W. Jia, D. Jia, T. Rodriguez, D. R. Evans, R. S. Meltzer, and W. M. Yen, *J. Lumin.*, **119-120**, 13 (2006).
- P. Boutinaud, E. Pinel, and R. Mahiou, *Opt. Mater.*, **30**, 1033 (2008).
- T. M. Mazzo, M. L. Moreira, I. M. Pinatti, F. C. Picon, E. R. Leite, L. I. V. Rosa, J. A. Varela, L. A. Perazolli, and E. Longo, *Opt. Mater.*, **32**, 990 (2010).
- Y. Inaguma, T. Tsuchiya, Y. Mori, Y. Imade, N. Sato, T. Katsumata, and D. Mori, *Thermochimica Acta*, **532**, 168 (2012).
- P. Boutinaud, P. Putaj, R. Mahiou, E. Cavalli, and A. Speghini, *Spectroscopy Letters*, **40**, 209 (2007).
- Shosuke Mochizuki, Fumito Fujishiro, and Seiko Minami, *J. Phys.: Condensed Matter*, **17**, 923 (2005).
- M. Capizzi and A. Frova, *Phys. Rev. Lett.*, **25**, 1298 (1970).
- S. Okamoto, H. Kobayashi, and H. Yamamoto, *J. Appl. Phys.*, **86**, 5594 (1999).
- S. H. Wemple, *Phys. Rev. B*, **2**, 2679 (1970).
- Xusheng Wang, Chao-Nan Xu, and Hiroshi Yamada, *Jpn. J. of Applied Physics*, **44**, L912 (2005).
- H. Yamamoto, S. Okamoto, and H. Kobayashi, *J. Lumin.*, **100**, 325 (2002).
- R. Fujiwara, H. Sano, M. Shimizu, and M. Kuwabara, *J. Lumin.*, **129**, 231 (2009).
- P. Boutinaud, L. Sarakha, R. Mahiou, E. Cavalli, M. Bettinelli, P. Dorenbos, and R. Mahiou, *J. Phys. D: Appl. Phys.*, **42**, 045106 (2009).
- P. Dorenbos and E. van der Kolk, *Proceedings of the society of photo-optical instrumentation engineers (SPIE)*, **6473**, 47313 (2007).
- W. Shan, W. Walukiewicz, J. W. Ager, K. M. Yu, H. B. Yuan, H. P. Xin, G. Cantwell, and J. J. Song, *Appl. Phys. Lett.*, **86**, 191911 (2005).
- I. Pelant and J. Valenta, *Luminescence Spectroscopy of Semiconductors*, Published to Oxford Scholarship Online, (2012) (DOI: 10.1093/acprof:oso/9780199588336.001.0001).
- Lin-Li Zhang, Chang-Xin Guo, Jun-Jing Zhao, and Jun-Tao Hu, *Chinese Physics Letters*, **22**, 1225 (2005).
- Chih-Cheng Yang, Suy-Yuh Cheng, Hsin-Yi Lee, and San-Yuan Chen, *Ceramics International*, **32**, 37 (2006).
- T. Pauporte, F. Pelle, B. Viana, and P. Aschehoug, *J. Phys. Chem. C*, **111**, 15427 (2007).
- W. M. Jadwisieniczak, H. J. Lozykowski, A. Xu, and B. Patel, *J. of Electronic Materials*, **31**, 776 (2002).
- A. S. Pereira, M. Peres, M. J. Soares, E. Alves, A. Neves, T. Monteiro, and T. Trindade, *Nanotechnology*, **17**, 834 (2006).
- Yong-Il Jung, Burn-Young Noh, Young-Seok Lee, Seong-Ho Baek, Jae Hyun Kim, and Il-Kyu Park, *Nanoscale Research Letters*, **7**, 43 (2012).
- Jihui Lang, Qiang Han, Jinghai Yang, Changsheng Li, Xue Li, Lili Yang, Yongjun Zhang, Ming Gao, Dandan Wang, and Jian Cao, *J. Appl. Phys.*, **107**, 074302 (2010).
- J. Iqbal, Z. Liu, H. Zhu, C. Pan, Y. Zhang, D. Yu, and R. Yu, *J. Appl. Phys.*, **106**, 083515 (2009).
- Z. M. Jarzebski and J. P. Marton, *J. of the Electrochem. Soc.*, **123**, 333C (1976).
- Do Hyung Park, Yang Hwi Cho, Young Rag. Do, and Byung Tae Ahn, *J. of the Electrochem. Soc.*, **153**, H63 (2006).
- R. S. Ningthoujam, V. Sudarsan, and S. K. Kulshreshtha, *J. Lumin.*, **127**, 747 (2007).
- Feng Gu, Shu Fen Wang, Meng Kai Lu, Guang Jun Zhou, Dong Xu, and Duo Rong Yuan, *J. Phys. Chem. B*, **108**, 8119 (2004).
- Feng Gu, Shu Fen Wang, Meng Kai Lu, Yong Xin Qi, Guang Jun Zhou, Dong Xu, and Duo Rong Yuan, *Opt. Mater.*, **25**, 59 (2004).
- D. F. Grabtree, *J. Phys. D: Appl. Phys.*, **8**, 2097 (1975).
- Zhizhong Yuan, Dongsheng Li, Zhizhong Liu, Xiaoqiang Li, Minghua Wang, Peihong Cheng, Peiliang Chen, and Deren Wang, *J. Alloys and Comp.*, **474**, 246 (2009).
- S. Dabboussi, H. Elhouichet, H. Ajlani, A. Moadhen, M. Oueslati, and J. A. Roger, *J. Lumin.*, **121**, 507 (2006).
- Weifeng Zhang, Junwang Tang, and Jinhua Ye, *J. Mater. Res.*, **22**, 1859 (2007).
- K. Goto, Y. Nakachi, and K. Ueda, *Thin Solid Films*, **516**, 5885 (2008).
- Zuoqiu Liang, Jinsu Zhang, Jiashi Sun, Xiangping Li, Lihong Cheng, Haiyang Zhong, Shaobo Fu, Yue Tian, and Baojiu Chen, *Physica B: Condens. Matter*, **412**, 36 (2013).
- Bingfu Lei, Bin Li, Haoran Zhang, Liming Zhang, Yan Cong, and Wenlian Li, *J. Electrochem. Soc.*, **154**, H623 (2007).
- Zuofeng Fu, Hyun Kyoung Yang, Byung Kee Moon, Byung Chun Choi, and Jung Hyun Jeong, *J. Nanoscience and Nanotechn.*, **11**, 1629 (2011).
- Zuofeng Fu, Wenhao Li, Shan Du, Hyun Kyoung Yang, and Jung Hyun Jeong, *J. Electrochem. Soc.*, **156**, J308 (2009).
- T. Nakamura, M. Shima, M. Yasukawa, and K. Ueda, *J. Sol-Gel Technol.*, **61**, 362 (2012).
- D. K. Patel, B. Rajeswari, V. Sudarsan, R. K. Vatsa, R. M. Kadam, and S. K. Kulshreshtha, *Dalton Trans.*, **41**, 12023 (2012).
- K. Ueda, T. Yamashita, K. Nakayashiki, K. Goto, T. Maeda, K. Furui, K. Ozaki, Y. Nakachi, S. Nakamura, M. Fujisawa, and T. Miyazaki, *Jpn. J. of Appl. Phys.*, **45**, 6981 (2006).

72. Z. Kotan, M. Ayvacikli, Y. Karabulut, J. Garcia-Guinea, L. Tormo, A. Canimoglu, T. Karali, and N. Can, *J. Alloys Comp.*, **581**, 101 (2013).
73. Qinzhuang Liu, Bing Li, Jianjun Liu, Hong Li, Zhongliang Liu, Kai Dai, Guangping Zhu, Peng Zhang, Feng Chen, and Jianming Dai, *Europhysics Letters*, **98**, 47010 (2012).
74. Y. Suzuki and M. Kakihana, *J. Am. Ceram. Soc.*, **92**, S168 (2009).
75. T. Yamashita and K. Ueda, *J. Solid State Chem.*, **180**, 1410 (2007).
76. Li Yuzhong and Zhou Xiaochun, *Adv. Mater. Res.*, **136**, 14 (2010).
77. Shi-Liu Fu, Tao Yin, and Fei Chai, *J. Inorganic Materials*, **22**, 647 (2007).
78. T. Ishigaki, A. Torisaka, K. Nomizu, P. Machusudan, K. Uematsu, K. Toda, and M. Sato, *Dalton Transactions*, **42**, 4781 (2013).
79. R. K. Swank, *Phys. Rev.*, **153**, 844 (1967).
80. Sanghyun Ju, Sunkook Kim, Saeed Mohammadi, David B. Janes, Young-Geun Ha, A. Facchetti, and T. J. Marks, *Appl. Phys. Lett.*, **92**, 022104 (2008).
81. V. Quemener, M. Alnes, L. Vines, P. Rauwel, O. Nilsen, H. Fjellvag, E. V. Monakhov, and B. G. Svensson, *J. Phys. D: Appl. Phys.*, **45**, 315101 (2012).
82. K. B. Sundaram and A. Khan, *J. Vac. Sci. Technol. A*, **15**, 428 (1997).
83. Electronic Materials: Science & Technology, *Photoelectrochemical Hydrogen Production*, Editors R. van de Krol and M. Gratzel, Springer, London.